Potential effects on effective attraction between probes diffusing in colloidal crystal

Luhui Ning ⬤,[1,2] Xiaoting Yu,[3] Xue Zhang,[3] Wei Liu,[3] Ke Chen,[4,5,6,*] Ning Zheng ⬤,[3,†]
Mingcheng Yang,[4,5,6,‡] and Peng Liu ⬤[3,§]

[1]*Beijing Key Laboratory of Optical Detection Technology for Oil and Gas, China University of Petroleum-Beijing, Beijing 102249, China*
[2]*Basic Research Center for Energy Interdisciplinary, College of Science, China University of Petroleum-Beijing, Beijing 102249, China*
[3]*School of Physics, Beijing Institute of Technology, Beijing 100081, China*
[4]*Beijing National Laboratory for Condensed Matter Physics and Laboratory of Soft Matter Physics,*
Institute of Physics, Chinese Academy of Sciences, Beijing 100190, China
[5]*School of Physical Sciences, University of Chinese Academy of Sciences, Beijing 100049, China*
[6]*Songshan Lake Materials Laboratory, Dongguan, Guangdong 523808, China*

Considering the significant influence of interparticle potentials on traditional depletion forces, we here employ computer simulations to investigate how varying potentials between particles affect the effective interaction of probes diffusing freely in a 2D colloidal crystal. Our results reveal that attractive potentials between the background particles and probes significantly modify the interprobe effective interactions, whereas long-range repulsive tails among the background particles have minimal impact. Furthermore, we observe contrary temperature dependencies of the effective force for soft and stiff repulsions between the background particles. These findings provide deeper insights into how direct interparticle potentials shape entropic-dominated effective forces mediated by colloidal crystals.

I. INTRODUCTION

Depletion force refers to an effective attraction between large mesoscopic objects mediated by a bath of smaller mesoscale particles (depletants) [1,2]. It provides a crucial avenue for directing self-assembly [3,4], and controlling the stability [5,6] and phase behavior [7,8] of complex fluids. The depletion attraction mainly arises from the gain in system entropy dominated by the depletants, by compressing the phase space of the large particles, and is therefore called an entropic force. While, direct interaction potentials between particles have been revealed to significantly influence the depletion force [9–13].

Given that the depletion-type entropic attraction is ubiquitous and paramount in shaping the equilibrium properties of large objects suspended in a fluid of smaller mesoscale particles, an interesting and opposite situation emerges when small mesoscopic probes move in a crystal composed of large colloidal particles. In a very recent work [14], we have shown that small purely-repulsive probes, diffusing freely in a two-dimensional fluctuating colloidal lattice whose constituents also interact repulsively with the probes, can experience effective attractions. This phenomenon is reminiscent of Cooper pairs of electrons in superconductors, where the background ions also maintain a stable and fluctuating lattice [15,16].

Furthermore, we found that the colloidal lattice background-induced effective attraction is entropically dominant. This novel entropic force arises from the fact that the background colloidal particles vibrating around the lattice sites can acquire more vibrational entropy by bringing smaller probes closer together, thereby decreasing the effective deformation of the crystalline lattice. Compared to the traditional depletion forces in fluid backgrounds, an unexplored fundamental issue is how direct interparticle potentials change the effective interactions between probes diffusing in a colloidal crystal.

In this work, we perform computer simulations to systematically study how interparticle potentials affect the entropy-originated effective interactions between the small probes in a 2D colloidal crystal background. In simulations, we consider different types of repulsive and attractive potentials to describe direct interactions between the large background particles and small probes, and tune the range and depth of the attractive well extensively. We find that, in general, the attractive potential between the background particle and probe significantly modifies the interprobe effective interaction. Additionally, we vary the long-range repulsion between the background particles while maintaining identical short-range hard-core repulsion. Our results indicate that the long-range repulsive tail has negligible influence on the interprobe effective attraction. Finally, we investigate the temperature dependence of the effective force for varying repulsive potentials between the background particles and find that soft and stiff repulsions can lead to opposite dependencies of the effective force on the system temperature.

---

*Contact author: kechen@iphy.ac.cn
†Contact author: ningzheng@bit.edu.cn
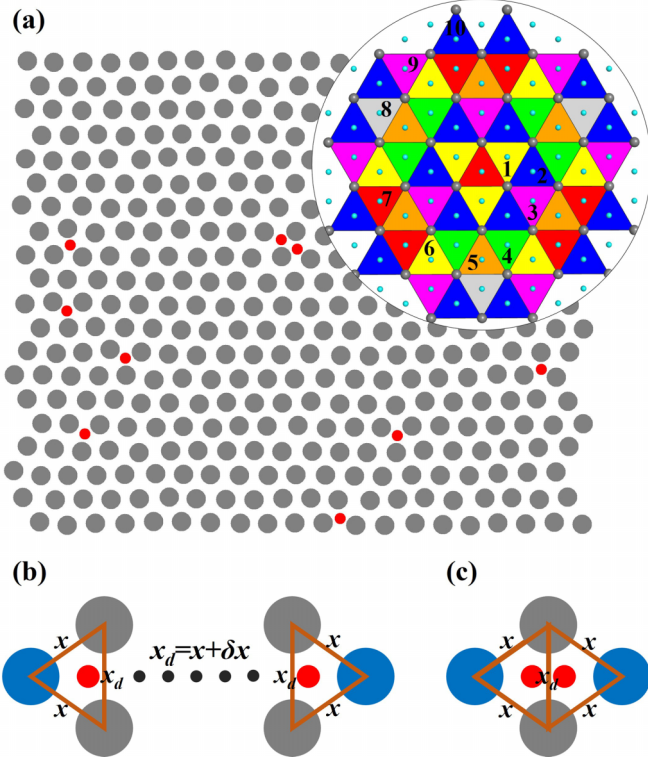‡Contact author: mcyang@iphy.ac.cn
§Contact author: liupeng@bit.edu.cn

FIG. 1. (a) Simulation snapshot of 9 red small probes diffusing in a crystalline lattice background with a lattice constant $L/\sigma_l = 1.052$, where the radius of the large background particles defines the basic length scale (1 unit). In the inset, a schematic diagram illustrates how neighboring cells are determined relative to the red triangle at the center. The large grey particles represent the background particles and the small cyan beads denote the centers of triangular cells. Neighbors from 1 to 10 are labeled with digits and different colors [14]. The schematic diagrams in (b) and (c) illustrate lattice distortion, where the bond length is elongated to $x_d = x + \delta x$ from x due to probe invasion. Furthermore, when two probe particles are situated in nearest-neighbor cells, two elongated bonds merge into one.

II. SIMULATION METHOD

In our simulations, we model the diffusion of several small tracers within a fluctuating two-dimensional lattice composed of 400 large particles, as shown in Fig. 1(a). The diameter of the large background particles is set to $\sigma_l = 2$, with the radius defined as the basic length scale (1 unit). The diameter of the tracers is set to one-fourth of this, $\sigma_s = 0.5$, consistent with the bidisperse polystyrene particles used in our previous experiments [14]. The interaction between particles is modeled using the Weeks-Chandler-Andersen (WCA) potential [17]:

$$U_{\text{WCA}}(r) = \begin{cases} 4\epsilon \left[\left(\frac{\sigma}{r} \right)^{2n} - \left(\frac{\sigma}{r} \right)^{n} \right] + \epsilon & r \leqslant r_c, \\ 0 & r > r_c. \end{cases} \quad (1)$$

This potential is derived from the Mie potential [18], a generalization of the Lennard-Jones potential, and has been modified to be purely repulsive [19]. Here, $\epsilon = k_B T$

represents the interaction intensity, and $r_c = 2^{1/n}\sigma$ is the cutoff radius, where the interaction diameters σ are σ_l, σ_s, and $(\sigma_l + \sigma_s)/2$ for large-large, small-small, and large-small particles, respectively. Unless stated otherwise, the stiffness coefficient is set as $n_{ll} = 12$ and $n_{ls} = 12$ for background-background and background-tracer particle interactions to model stronger short-range repulsion [20,21], while $n_{ss} = 2$ is used for tracer-tracer interactions to describe relatively softer repulsion. The selection of the stiffness coefficient is based on empirical interactions from previous experiments [14,22], which are detailed in the Supplemental Material [23]. The dynamics of all particles follow the overdamped Langevin equation $\gamma \mathbf{v} = \mathbf{F}_r + \boldsymbol{\eta}$ under periodic boundary conditions, with γ the friction coefficient, $\mathbf{F}_r$ the steric interaction force, and $\boldsymbol{\eta}$ the Gaussian distributed stochastic force having $\langle \boldsymbol{\eta} \rangle = 0$ and $\langle \eta_\alpha(t)\eta_\beta(t') \rangle = 2k_B T \gamma \delta_{\alpha\beta} \delta(t - t')$.

The background particles initially form a hexagonal arrangement with a lattice constant of $L/\sigma_l = 1.052$ and an area fraction of 0.82. For roughly equivalent hard disks, the lattice is only slightly perturbed by thermal fluctuations, without defects. The tracers are initially distributed randomly. The equations of motion are integrated with a time step $\Delta t = 10^{-5} \times \gamma \sigma_l^2 / 2\epsilon$ and 10^8 steps are performed to relax the initialized system, followed by 3×10^9 steps to compute the relevant physical quantities. To measure the probability of finding a tracer pair in triangular lattice cells with different separations, we use the same scheme as in our previous study [14] [see the inset of Fig. 1(a)]. For any reference cell in the lattice, indicated by the red cell at the center, we identify equivalently positioned neighboring cells based on their center-to-center distance from the reference cell and highlight them with identical colors. The relative probability of finding a tracer pair in mth nearest neighbor cell is then described by

$$P(m) = \frac{\sum_{i \in m} \frac{1}{g_{ss}(r)} / \sum_{i \in 1 \cdots 10} \frac{1}{g_{ss}(r)}}{D(m) / \sum_{m=1}^{10} D(m)}. \quad (2)$$

Here, the probability is normalized by the cell degeneracy $D(m)$. To eliminate the effect of direct interactions between the probes, a factor of $1/g_{ss}(r)$ is multiplied to the countings of probe pairs with separation r, where $g_{ss}(r)$ is the radial distribution function of the probes measured in dilute solutions without the background lattice.

We would like to highlight that the discrete relative probability $P(m)$ at various cell separations, rather than the traditionally used radial distribution function $g_{ss}(r)$, correctly captures the effective interactions between tracers within a crystalline background. The conventional tracer $g_{ss}(r)$ is typically calculated under the assumption of isotropic and homogeneous conditions, which may result in misleading indications of artificial attraction when applied to a lattice background. A comprehensive explanation of this distinction is provided in the Supplemental Material of Ref. [14] by Liu *et al.* Furthermore, $P(0)$ is not displayed in this work because two tracers hardly occupy the same triangular cell, as this would require very large lattice deformation.
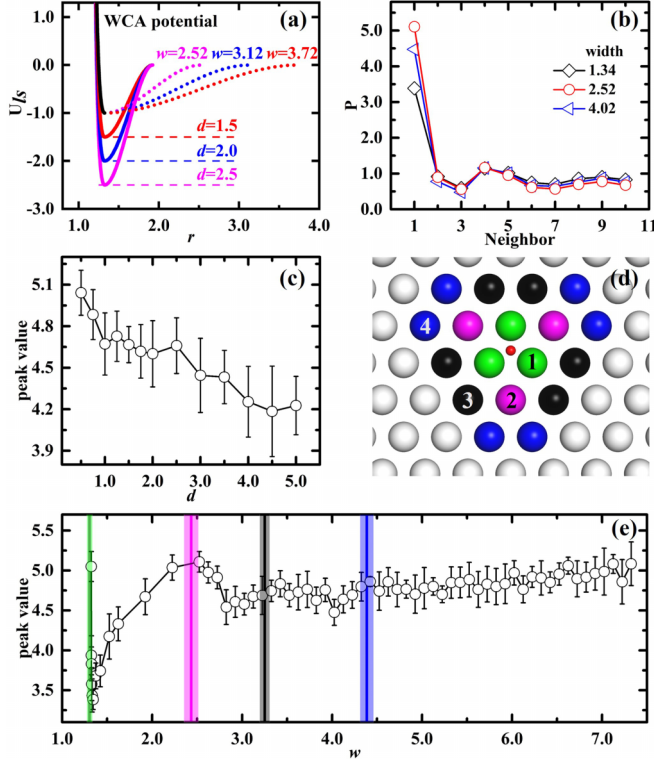
FIG. 2. (a) The potential interaction between the large background particle and small tracer is modelled by combining the WCA potential with an attractive tail. (b) Relative probabilities of finding tracer pairs in neighboring cells from 1 to 10, with peak values depicted across various (c) potential depths and (e) widths. (d) Schematic diagram illustrating neighboring large background particles, enumerated 1st to 4th, relative to the red small tracer, distinguished by digits and different colors. Colored vertical lines with shadows in (e) signify average distances with associated standard errors between the diffusing tracer and the four types of neighboring large particles. Here, the basic units of energy and length are k_BT and $\sigma_l/2$, respectively.

III. RESULTS AND DISCUSSION

A. The effects of potential between background particle and probe

1. Connecting the purely repulsive WCA potential with an attractive tail

In our previous work [14], all interparticle interactions employed in the simulations are considered repulsive in order to mimic like-charge couplings between colloidal particles. Nevertheless, another more typical potential interaction between colloidal particles often contains a hard-core repulsion together with an attractive tail, as in the recent experiment by Mondal *et al.* [24]. To model this properly, we incorporate an adjustable attractive function into the unchanged WCA repulsion. This approach allows us to describe the interactions between the large background particles and small tracers flexibly. In Fig. 2(a), several potential curves are depicted with the stiffness parameter of the WCA potential set to $n_{ls} = 12$. The width and depth of the attractive part are adjusted using fitting cubic functions of the form $U_{ls}(r) = Ar^3 + Br^2 + Cr + D$. The parameters A, B, C, and

D, corresponding to various widths and depths, are listed in the Supplemental Material [23]. When adjusting the potential depth [colored lines in Fig. 2(a)], we fixed the potential width at $w = 2^{\frac{1}{n_{ls}}}(\sigma_l + \sigma_s)/2 + 0.3\sigma_l$, where $2^{\frac{1}{n_{ls}}}(\sigma_l + \sigma_s)/2$ represents the cutoff radius of the purely WCA repulsive interaction between background and tracer particles, and $0.3\sigma_l$ corresponds to the additional width of the attractive part. Similarly, when adjusting the potential width [colored dotted lines in Fig. 2(a)], we kept the potential depth constant at $d = \epsilon$. Meanwhile, the stiffness coefficient is set to $n_{ll} = 12$ for background-background particle interactions, and a repulsive soft potential is used to describe the interactions between small tracers. The tracer-tracer interactive potential is derived from experiments conducted in dilute solutions without any large background particles [14] (see Supplemental Material [23]). With this type of potentials, Fig. 2(b) displays the relative probabilities of finding tracer pairs in neighboring cells from 1 to 10, which are similar to the observation obtained in our previous work [14]. The peak values, $P(1)$ in [Eq. (2)], suggest that, despite the existence of attraction between the large particles and small probes, the fluctuating lattice can cause two probes to locate in neighboring triangular cells, indicating the presence of an effective attraction between the probes. The microscopic mechanism is illustrated in Figs. 1(b) and 1(c), where the presence of a tracer elongates the bond closest to it from x to $x_d = x + \delta x$, incurring a penalty for elastic free energy. The system then minimizes its total free-energy cost by moving two distant tracers into neighboring cells that share an elongated bond.

When adjusting the potential depth, Fig. 2(c) illustrates a monotonically decreasing peak value. As per previous findings [14], a pure hard-core repulsion typically induces significant attraction between tracers driven by entropy. Therefore, it is reasonable to anticipate that the decrease in the peak value with the potential depth is due to the increasing importance of potential energy in competing with entropy. On one hand, from Fig. 1(c), the effective inter-tracer attraction stems from minimizing the free-energy cost, leading to the merging of two elongated bonds into one. On the other hand, the introduction of an attractive potential creates a trough in the triangular center of the potential energy landscape, encouraging tracers to diffuse toward the center of the triangular cell. As a result, deepening the attractive well decreases the entropy gain from minimizing the lattice deformation and thus reduces the peak value (effective attraction).

A nonmonotonic change in the peak value occurs with increasing the attractive potential width [Fig. 2(e)], in which a steep drop in $P(1)$ is noticeable when the pure hard-core repulsive potential is combined with a short-range attractive term. This drop is similar to the depth dependence in Fig. 2(c). The key distinction lies in the more localized and steeper nature of the attraction landscape, such that the probe more likely stays around the center of the trough area, thereby intensifying the decrease of $P(1)$. As the potential width increases, and the potential energy landscape becomes smoother, the peak value of the relative probability gradually recovers to its highest point. To illustrate this behavior, we categorize neighboring large particles relative to the reference red tracer in the center triangular unit based on their center-to-center distances, as shown in Fig. 2(d). The average distances,

along with standard errors, between the diffusing tracer and these fluctuating background particles are represented by colored vertical lines in Fig. 2(e). Interestingly, the potential width corresponding to the recovery of the highest $P(1)$ precisely aligns with the average distance between the diffusing tracer and the second-neighboring background particles. This suggests that the slightly long-ranged attractive interaction between the tracer and the second-neighboring large particles significantly smooths the potential landscape surrounding the tracers. Further increase in the potential width may induce minor fluctuations in the peak value, meaning a diminishing effect of the long-ranged attractive term on the inter-tracer attractions.

2. A LJ–like potential with a natural truncation

In colloidal simulations, the Lennard-Jones (LJ) potential has been extensively used. Note that the potential energy curves depicted in Fig. 2(a) are different from the LJ potential, since the hard-core repulsion of the LJ potential simultaneously experiences a change when tuning its attractive well. To be complete, we also investigate the potential dependence of the effective interaction by using an LJ–like potential proposed by Frenkel *et al.* [25–29] to characterize interactions between background and tracer particles,

$$\phi(r) = d\alpha \left[\left(\frac{\sigma}{r} \right)^2 - 1 \right] \left[\left(\frac{w}{r} \right)^2 - 1 \right]^2, \quad (3)$$

with

$$\alpha = 2 \left(\frac{w}{\sigma} \right)^2 \left[\frac{3}{2 \left(\left(\frac{w}{\sigma} \right)^2 - 1 \right)} \right]^3. \quad (4)$$

Here, the benchmark potential depth and width are specified as $d = \epsilon$ and $w = 1.15\sigma_l$, respectively. By construction, the range of this LJ–like potential is exactly finite and hence has a natural truncation instead of a hard truncation, as plotted in Figs. 3(a) and 3(b). Here, purely repulsive WCA potential is employed to model interactions between background-background and tracer-tracer particles, with $n_{ll} = 12$ and $n_{ss} = 2$. Figures 3(c) and 3(d) show the corresponding peak values of relative probability of the probe pair. Interestingly, the behavior observed differs from that shown with the fitted cubic functions [Fig. 2(a)], due to significant differences in potential morphology and second derivatives between Figs. 2(a) and 3(a). In Fig. 2(a), adjusting the attractive tail leaves the WCA part fixed. However, in Fig. 3(a), both the repulsive and attractive components change simultaneously, where the repulsive part becomes steeper as the potential depth increases, while a longer attractive range smoothens the repulsion, as illustrated in Fig. 3(b).

For the WCA and attractive tail potential, the deeper trough at the triangular center of the potential energy landscape encourages tracers to diffuse toward the center, hindering elongated bond sharing and reducing free-energy savings. This results in a decrease in peak values with increasing potential depth, as shown in Fig. 2(c). In contrast, the LJ–like potential in Fig. 3(a) changes both its repulsive and attractive parts simultaneously, where a steeper repulsive interaction emerges when increasing the attraction depth. Since the lattice-induced inter-tracer interactions are driven primar-
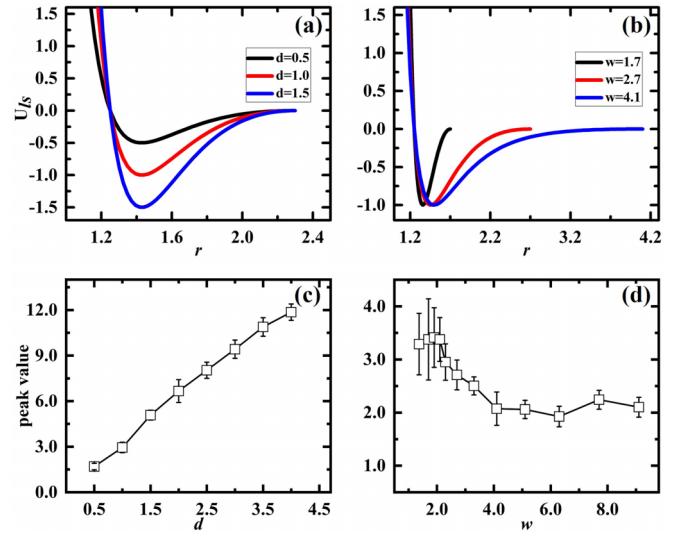

FIG. 3. The Frenkel potential, characterized by different (a) depths and (b) widths, models interactions between large background and small tracer particles. Peak values of relative probabilities for finding a tracer pair in neighboring cells are depicted across various (c) potential depths and (d) widths.

ily by entropy through hard-core interactions [14], the larger anharmonicity in the LJ–like potential enhances the effective attraction. This leads to the increase in peak values with the LJ–like potential depth in Fig. 3(c), which is in stark contrast to the trend seen in Fig. 2(c). Similarly, in Fig. 3(b), the steepness of the repulsive part, and consequently the inter-tracer attraction [Fig. 3(d)], decreases as the attractive potential width increases.

B. The effects of potential between large background particles

1. A Yukawa–type long-range repulsive potential

After the background particle-probe potentials have been systematically investigated, we now focus on the potential interactions between the lattice background particles. Here, we only consider purely repulsive background particles that can form a stable and loose crystal in which the probes freely diffuse. To adjust this repulsive potential, we combine the unaltered WCA hard-core potential [Eq. (1)] with various Yukawa–type long-range repulsions, while keeping the lattice constant fixed:

$$U_{\text{WCA}}(r) + \epsilon \left(\frac{\sigma_l}{r} \right) \exp \left[-\lambda \left(\frac{r - \sigma_l}{\sigma_l} \right) \right]. \quad (5)$$

Here, the steepness and range of the Yukawa potential depend sensitively on the screening parameter λ. Figure 4(a) depicts several such combined potential curves, with the stiffness of the WCA part set as $n_{ll} = 12$ and the interaction diameter as $\sigma_l = 2$. The stiffness coefficient is set to $n_{ls} = 12$ for background-tracer particle interactions, and the interactions between small tracers are consistent with those in Fig. 2. The constant peak value of the relative tracer pair probabilities in neighboring cells [Fig. 4(b)] implies that the steepness of the long-range soft repulsion, determined by λ, exerts minimal impact on the inter-tracer effective interactions. This
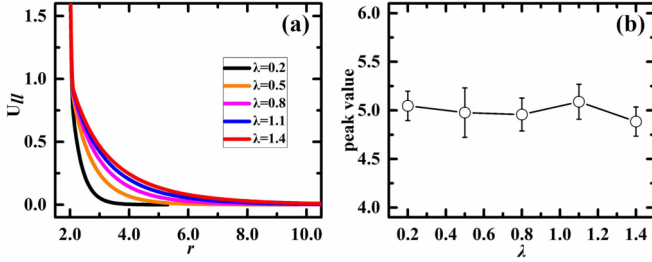
FIG. 4. (a) Yukawa potential with different screening parameters λ describes the long-range interactions among the large background particles, combined with a fixed WCA potential for $r < 2^{\frac{1}{n_{ll}}} \sigma_l$. (b) Peak values of the relative tracer pair probabilities in neighboring cells versus the screening parameter λ.

observation contrasts with previous experimental studies [14], where the charge quantity around colloidal surfaces directly influenced the lattice constant. In our simulations, however, both the lattice constant and the underlying WCA stiffness remain unchanged. This finding again highlights the importance of the short-range repulsion and hence the entropic contribution in the lattice-induced interprobe effective interactions.

2. The contrasting temperature dependencies of the effective interaction for soft and stiff repulsions

Finally, we study the dependence of the interprobe effective attraction on the system temperature. By adjusting the hard-core repulsion between large background particles, we observe a counterintuitive phenomenon where the bound tracers may not necessarily dissociate upon heating. As shown in Fig. 5(a), the peak value increases with the temperature, indicating a more pronounced aggregation of the tracer pairs. Conversely, Fig. 5(b) demonstrates a weakening inter-tracer attraction when raising the temperature. This disparity stems from the differing stiffness values: $n_{ll} = 18$ in Fig. 5(a) compared to $n_{ll} = 6$ in Fig. 5(b). In the current setup, the attraction between tracers mainly arises from entropic effects, where the tracers restrict the vibrations of the crystal lattice. Consequently, at higher temperatures, the

increasing lattice vibration strengthens the binding between the tracers, as there is a greater entropy gain for the lattice with higher vibrational amplitudes. However, a softer lattice with a lower WCA stiffness ($n_{ll} = 6$) results in the expected disintegration-on-heating behavior, since in this case the background lattice may gain additional configuration entropy through local deformations. The attractive interaction diminishes as the temperature rises from $0.5k_BT$ to $0.9k_BT$, as depicted in Fig. 5(b). At higher temperatures, the softer lattice becomes significantly distorted and develops defects. Neither the $g(r)$ method, which assumes isotropic and homogeneous conditions, nor the binning approach, which assumes a defect-free lattice as shown in Fig. 1(a), can accurately capture the defective lattice-induced interactions between tracer pairs. Overall, the potential stiffness between the background particles directly influences the temperature dependence of the effective interprobe attraction in a fluctuating lattice background.

IV. CONCLUSIONS

We explore the potential effects on the lattice-induced inter-tracer attraction, considering the interactions between the background particles and small probes, as well as those among large background particles. Our findings reveal that the attractive interaction between background and tracer particles leads to noticeable changes in the probability of finding tracer pairs in nearest-neighboring cells. Nevertheless, the inter-tracer effective attraction still is predominantly governed by the hard-core repulsion. Moreover, we observe that a long-range soft repulsion between the background particles does not significantly affect the inter-tracer effective interaction, given that there is an identical short-ranged hard-core repulsion. Noticeably, the change in the stiffness of the hard-core repulsion between the background particles is found to directly dictate the thermal response of the inter-tracer attraction. The present study unveils the subtle competition between the potential energy and entropy in the lattice-induced effective interactions between freely diffusing tracers, thus providing a comprehensive understanding of its origin and properties.
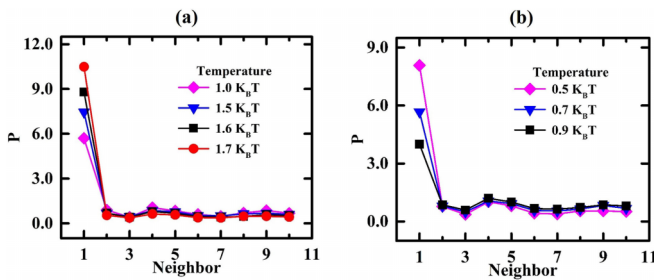
FIG. 5. (a) Relative probabilities of finding a tracer pair in neighboring cells from 1 to 10 at varying temperatures, with stiffness parameters set to $n_{ll} = 18$, $n_{ls} = 12$, and $n_{ss} = 2$. (b) Relative probabilities at different temperatures, with the same simulation parameters as (a) except for a lower stiffness coefficient of $n_{ll} = 6$.

[1] S. Asakura and F. Oosawa, J. Polym. Sci. **33**, 183 (1958).

[2] A. Vrij, Pure Appl. Chem. **48**, 471 (1976).

[3] S. Sacanna, W. T. M. Irvine, P. M. Chaikin, and D. J. Pine, Nature (London) **464**, 575 (2010).

[4] G. Meng, N. Arkus, M. P. Brenner, and V. N. Manoharan, Science **327**, 560 (2010).

[5] G. H. Koenderink, G. A. Vliegenthart, S. G. J. M. Kluijtmans, A. van Blaaderen, A. P. Philipse, and H. N. W. Lekkerkerker, Langmuir **15**, 4693 (1999).

[6] K. Lin, J. C. Crocker, A. C. Zeri, and A. G. Yodh, Phys. Rev. Lett. **87**, 088301 (2001).

[7] M. Adams, Z. Dogic, S. L. Keller, and S. Fraden, Nature (London) **393**, 349 (1998).

[8] A. Stradner, H. Sedgwick, F. Cardinaux, W. C. K. Poon, S. U. Egelhaaf, and P. Schurtenberger, Nature (London) **432**, 492 (2004).

[9] J. Y. Walz and A. Sharma, J. Colloid Interface Sci. **168**, 485 (1994).

[10] O. Mondain-Monval, F. Leal-Calderon, J. Phillip, and J. Bibette, Phys. Rev. Lett. **75**, 3364 (1995).

[11] A. A. Louis, E. Allahyarov, H. Löwen, and R. Roth, Phys. Rev. E **65**, 061407 (2002).

[12] S. A. Egorov, Phys. Rev. E **70**, 031402 (2004).

[13] T. N. Shendruk, M. Bertrand, J. L. Harden, G. W. Slater, and H. W. de Haan, J. Chem. Phys. **141**, 244910 (2014).

[14] P. Liu, L. Ning, Y. Zong, F. Ye, M. Yang, and K. Chen, Phys. Rev. Lett. **129**, 018002 (2022).

[15] J. Bardeen, L. N. Cooper, and J. R. Schrieffer, Phys. Rev. **108**, 1175 (1957).

[16] J. Linder and A. V. Balatsky, Rev. Mod. Phys. **91**, 045005 (2019).

[17] J. D. Weeks, D. Chandler, and H. C. Andersen, J. Chem. Phys. **54**, 5237 (1971).

[18] G. Mie, Ann. Phys. **316**, 657 (1903).

[19] D. Lüsebrink, M. Yang, and M. Ripoll, J. Phys.: Condens. Matter **24**, 284132 (2012).

[20] J. F. M. Lodge and D. M. Heyes, J. Chem. Soc. Faraday Trans. **93**, 437 (1997).

[21] J. F. M. Lodge and D. M. Heyes, Mol. Simul. **23**, 203 (1999).

[22] W. Chen, S. Tan, T.-K. Ng, W. T. Ford, and P. Tong, Phys. Rev. Lett. **95**, 218301 (2005).

[23] See Supplemental Material at http://link.aps.org/supplemental/10.1103/PhysRevE.110.044607 for additional experimental and simulation details, which includes Refs. [2,3].

[24] M. Mondal and R. Ganapathy, Phys. Rev. Lett. **129**, 088003 (2022).

[25] X. Wang, S. Ramírez-Hinestrosa, J. Dobnikar, and D. Frenkel, Phys. Chem. Chem. Phys. **22**, 10624 (2020).

[26] J. F. Lutsko and C. Schoonen, Phys. Rev. E **102**, 062136 (2020).

[27] B. Cheng and D. Frenkel, Phys. Rev. Lett. **125**, 130602 (2020).

[28] W.-B. Wang and M. Kambara, AIP Adv. **11**, 085119 (2021).

[29] P. Vélez, G. L. Luque, D. E. Barraco, A. A. Franco, and E. P. Leiva, Comput. Mater. Sci. **209**, 111409 (2022).